

Boosting dark matter searches at muon colliders with Machine Learning: the mono-Higgs channel as a case study

MOHAMED BELFKIR,^{1,*} ADIL JUEID,^{2,†} and SALAH NASRI^{1,3,‡}

¹*Department of physics, United Arab Emirates University, Al-Ain, UAE*

²*Particle Theory and Cosmology Group, Center for Theoretical Physics of the Universe,*

Institute for Basic Science (IBS), 34126 Daejeon, Republic of Korea

³*The Abdus Salam International Centre for Theoretical Physics, Strada Costiera 11, I-34014, Trieste, Italy*

The search for dark-matter (DM) candidates at high-energy colliders is one of the most promising avenues to understand the nature of this elusive component of the universe. Several searches at the Large Hadron Collider (LHC) have strongly constrained a wide range of simplified models. The combination of the bounds from the LHC with direct-detection experiments exclude the most minimal scalar singlet DM model. To address this, Lepton portal DM models are suitable candidates where DM is predominantly produced at lepton colliders since the DM candidate only interacts with the lepton sector through a mediator that carries a lepton number. In this work, we analyse the production of DM pairs in association with a Higgs boson decaying into two bottom quarks at future muon colliders in the framework of the minimal lepton portal DM model. It is found that the usual cut-based analysis methods fail to probe heavy DM masses for both the resolved (where the decay products of the Higgs boson can be resolved as two well-separated small- R jets) and the merged (where the Higgs boson is clustered as one large- R jet). We have then built a search strategy based on Boosted-Decision Trees (BDTs). We have optimised the hyperparameters of the BDT model to both have a high signal-to-background ratio and to avoid overtraining effects. We have found very important enhancements of the signal significance with respect to the cut-based analysis by factors of 8–50 depending on the regime (resolved or merged) and the benchmark points. Using this BDT model on a one-dimensional parameter space scan we found that future muon colliders with $\sqrt{s} = 3$ TeV and $\mathcal{L} = 1 \text{ ab}^{-1}$ can exclude DM masses up to 1 TeV at the 95% CL.

arXiv:2309.11241v1 [hep-ph] 20 Sep 2023

* m_belfkir@uaeu.ac.ae

† adiljueid@ibs.re.kr

‡ snasri@uaeu.ac.ae; salah.nasri@cern.ch

I. INTRODUCTION

Weakly interacting massive particles (WIMPs) are suitable candidates which extend the Standard Model (SM) in order to solve the dark-matter (DM) problem [1–4]. In particular WIMPs of mass of about 100 GeV yield a DM density of $\Omega_{\text{DM}}h^2 = 0.1198 \pm 0.0015$ in agreement with the PLANCK observation [5]. On the other hand, WIMPs can be connected to other problems like the hierarchy problem, baryon asymmetry in the universe or the nature of neutrino mass generation mechanism. The understanding of the nature of WIMPs has driven many searches in direct detection, indirect detection and collider experiments. At the Large Hadron Collider (LHC), the ATLAS and CMS collaborations have carried several searches in channels dubbed as mono- X , *i.e.* channels where a visible particle recoils against a large transverse missing energy (E_T^{miss}). Unfortunately all these searches were unsuccessful to find any interesting signal beyond the expected SM backgrounds and model-independent bounds were put on the DM mass versus the production cross section. On the other hand, strong bounds from direct detection experiments were also imposed as a consequence of the absence of new DM signals [6, 7]. By combining the results from both collider and direct detection experiments, we can narrow down the range of plausible beyond the SM scenarios aimed at addressing the DM problem. While the constraints from direct-detection experiments can be circumvented if the DM candidate is a right-handed fermion for example¹, earlier and current collider searches strictly constrain minimal models (see for example a recent reinterpretation of multijet+ E_T^{miss} searches [11]). To avoid these issues, there is a possibility that the DM candidate couples *solely* to the lepton sector of the SM. In such scenarios the DM is called leptophilic and the models that contain such a DM are called lepton portal models. In the case of fermionic DM candidates, the interaction Lagrangian resembles to that of slepton-lepton-neutralino interaction in supersymmetric models. The most minimal choice in this case would consist of extending the SM with only two $SU(2)_L$ singlets. The phenomenology of these minimal models has been studied in Refs. [12–19].

The LHC programme for DM searches is still not over with the possibility to probe DM masses as high as 0.5–2 TeV depending on the model. However, there is *a priori* no reason to not consider alternative future collider experiments which can both achieve high center-of-mass energies and provide very clean environments. Muon colliders are expected to provide both these characteristics at relatively low costs as compared to *e.g.* future circular hadron colliders (FCC-hh). There is a growing interests on the physics potential of muon colliders since they can probe new physics beyond the SM at very high scales [20–22]. There are many reasons for this interest. First, muon colliders can achieve small signal-to-background ratios as compared to the LHC. Second, given that muons are elementary particles, the center-of-mass energy required to achieve the same beam-level cross section is always orders of magnitude smaller than that in pp collisions. Finally, at energies much higher than the production threshold of heavy resonances, muon colliders become vector-boson colliders where the dominant production channels occur through vector-boson fusion (VBF) [23, 24] in which case many processes in beyond the SM are free of backgrounds. Extensive studies of both the SM and beyond the SM have been carried in the literature [19, 25–63].

The main production mechanism of DM at muon colliders is through mono- X channels. For the case of muon colliders, the phenomenology of DM in mono-photon, and mono-muon channels has been performed at the parton level in Ref. [28]. The mono-Higgs channel is however very unique since the SM Higgs boson is the only particle that can be produced from the interaction with the dark sector due to the smallness of the muon-Yukawa coupling unlike the mono-photon channel which can also be produced from Initial-State Radiation (ISR). Therefore, the mono-Higgs channel can be a very important channel to study the characteristics of the underlying model. The mono-Higgs channel has been suggested sometime ago in Ref. [64] and studied extensively for both hadron colliders and lepton colliders (see *e.g.* Refs. [65–77]). In Ref. [19] a comprehensive analysis of the DM production within minimal lepton portal DM model has been done including the mono-Higgs production. This article presents a first study in a serie of upcoming works where we fully analyse the most prominent channels for DM at muon colliders and using state-of-art tools. In this study, we analyse the production of DM in association with a Higgs boson decaying into bottom quarks at future muon colliders using center-of-mass energy of 1 TeV and a total luminosity of 1 ab^{-1} . The final state consists of

¹ Studies have shown that right-handed fermion singlets interact with the nucleons solely via loops and therefore their interaction rates are small thanks to loop suppression factors even for couplings of order one (see *e.g.* Refs. [8–10]).

jets and missing energy. We use both the resolved regime where the decay products of the Higgs boson are two well-separated jets and the merged regime where the Higgs boson is identified with a single large- R jet. First we use cut-based analysis inspired from the searches of DM in the mono-Higgs channel that have been carried by the ATLAS and CMS collaborations [78, 79]. It is found that cut-based search strategies are not sensitive to heavy DM masses. We then employ a boosted-decision Tree (BDT) algorithm as implemented in XGBOOST to further improve the signal-to-background ratio. We found that the BDT model leads to very important enhancements of the significance by large factors of 8–50 depending on the analysis region and the DM mass. We find that DM masses up to 1 TeV can be probed at future muon colliders if one employs BDTs.

The rest of this paper is organised as follows. In section II we briefly describe the theoretical setup including the benchmark points and the scanning procedure. We define the technical setup along with the discussion about the signal and the background cross sections and the object definitions at the detector level in section III. Section IV is devoted to a detailed cut-based analysis. We then study the sensitivity reach using the BDT model in section V. We conclude in section VI.

II. THEORETICAL SETUP

In this section, we discuss the theoretical setup used in this work. We briefly introduce the model, its particle content and its parameters. We close this section by a discussion of the benchmark points and the scanning procedure to be used in the collider analysis.

A. The model

We extend the SM by two $SU(2)_L$ gauge-singlet fields: a charged scalar (S) and a right-handed fermion (N_R). The quantum numbers of these new states are shown below

Field	$SU(3)_c$	$SU(2)_L$	$U(1)_Y$	Z_2
S	$\mathbf{1}$	$\mathbf{1}$	+2	−1
N_R	$\mathbf{1}$	$\mathbf{1}$	0	−1

TABLE I. The new particles of the model and their representation under $SU(3)_c \otimes SU(2)_L \otimes U(1)_Y \otimes Z_2$.

In this setup, we have introduced an accidental discrete symmetry (Z_2) under which the new particles are odd while all the SM particles are even. In this case, the right-handed fermion, being neutral particle, is a suitable candidate for DM, assuming it is lighter than the singlet scalar. We furthermore assume that the charged scalar singlet carries a lepton number which therefore implies that it only interacts with the SM charged leptons (right-handed leptons in particular). The resulting interaction would be similar to the case of slepton-neutralino-lepton in supersymmetric theories with the exception that here we only have one *slepton* particle that interacts with all the lepton generations. Under these assumptions, the most general Lagrangian is given by

$$\mathcal{L} = \mathcal{L}_S + \mathcal{L}_N + \mathcal{L}_{SN} - V(\Phi, S), \quad (1)$$

where \mathcal{L}_S represents the kinetic term for the charged scalar singlet, given by

$$\begin{aligned} \mathcal{L}_S &= (\mathcal{D}^\mu S)^\dagger (\mathcal{D}_\mu S) = (\partial^\mu S)^\dagger (\partial_\mu S) - (eA^\mu - e \tan \theta_W Z^\mu) S^\dagger \overleftrightarrow{\partial}_\mu S \\ &+ e^2 A_\mu A^\mu S^\dagger S + e^2 \tan^2 \theta_W Z_\mu Z^\mu S^\dagger S - 2e^2 \tan \theta_W A_\mu Z^\mu S^\dagger S, \end{aligned} \quad (2)$$

Here, in the first line, the first term refers to the kinetic energy of S , while the second term represents the triple interaction of S with the photon and the Z boson. The second line illustrates the quartic interaction of S with the γ/Z . In equation 2, we have $e = \sqrt{4\pi\alpha_{\text{EM}}}$ as the electric charge, θ_W denoting the Weinberg

Benchmark scenario	BP1	BP2	BP3	BP4
<i>Parameters</i>				
M_{N_R} (GeV)	50	200	598	1000
M_{H^\pm} (GeV)	500	500	600	1500
Y_e	10^{-4}	5×10^{-4}	10^{-3}	5×10^{-3}
Y_μ	2.8	1.6	1	2
Y_τ	5×10^{-2}	5×10^{-1}	5×10^{-1}	2
λ_3	4	5	5	6

TABLE II. Benchmark points used for the differential distributions in this analysis. More details can be found in Ref. [19].

weak mixing angle, and $A\overset{\leftrightarrow}{\partial}_\mu B \equiv A(\partial_\mu B) - (\partial_\mu A)B$. The notation $\mathcal{L}_N + \mathcal{L}_{SN}$ refers to the Lagrangian of the right-handed fermion and its interaction with S , which can be expressed as follows:

$$\mathcal{L}_N + \mathcal{L}_{SN} \equiv i\bar{N}_R \not{\partial} N_R^c + \frac{1}{2}M_N \bar{N}_R N_R^c + \left(Y_\ell \bar{\ell}_R^c N_R S + \text{h.c.} \right), \quad (3)$$

where M_N is the mass of the N_R particle and $Y_{\ell, \ell=e, \mu, \tau}$ are assumed to be real-valued couplings. In the last term, the sum over the lepton generations is implicit. Finally, the scalar potential is given by

$$V(\Phi, S) = -m_{11}^2 |\Phi^\dagger \Phi| + m_{22}^2 |S^\dagger S| + \lambda_1 |\Phi^\dagger \Phi|^2 + \lambda_2 |S^\dagger S|^2 + \lambda_3 |\Phi^\dagger \Phi| |S^\dagger S|, \quad (4)$$

where Φ is the SM Higgs doublet:

$$\Phi \equiv \begin{pmatrix} G^+ \\ \frac{1}{\sqrt{2}}(v + h + iG^0) \end{pmatrix},$$

and $v = \sqrt{2G_F}$ representing the vacuum expectation value (VEV), while G^0 and G^+ correspond to the Nambu-Goldstone bosons responsible for forming the longitudinal polarizations of the Z and W bosons, respectively. Following the electroweak symmetry breaking, we are left with three scalars: the CP-even scalar, identified as the 125 GeV Higgs boson, and a pair of charged scalars denoted as H^\pm in the subsequent discussion. Their tree-level masses are determined by:

$$M_{H_{SM}}^2 = \lambda_1 v^2 = -2m_{11}^2, \quad M_{H^\pm}^2 = m_{22}^2 + \frac{1}{2}\lambda_3 v^2. \quad (5)$$

In addition to the SM parameters, this model has seven more parameters defined by

$$\{M_{H^\pm}, M_{N_R}, \lambda_2, \lambda_3, Y_e, Y_\mu, Y_\tau\}. \quad (6)$$

The model is subject to various theoretical and experimental constraints. In this study, we take into account constraints from the stability of the scalar potential, unitarity of the scattering amplitudes, bounds from Higgs boson decays and lepton flavour violation. Additionally, we account for the constraints associated with the dark matter relic density and the direct detection experiments. Finally recasting the searches of sleptons and neutralinos at the LHC implies that mediator masses less than 400 GeV are excluded. For more details, we refer the interested reader to Refs. [16, 19].

B. Benchmark points and scanning procedure

We will start by examining four benchmark points, as shown in table II and have been previously considered in Ref. [19]. The illustration of the differential distributions and the performance of our algorithms will be discussed in great detail for these benchmark scenarios. Interestingly, the model predicts very simple relations

	$\sqrt{s_{\mu\mu}}$ [TeV]	3	10	30
$\sigma \times \text{BR}$ [fb] (N_{events})	BP1	6.70×10^1 (6.70×10^4)	1.02×10^0 (1.02×10^4)	3.67×10^{-2} (3.67×10^3)
	BP2	1.02×10^1 (1.02×10^4)	0.31×10^0 (0.31×10^4)	1.12×10^{-2} (1.12×10^3)
	BP3	0.82×10^0 (0.82×10^3)	0.47×10^{-1} (0.47×10^3)	1.81×10^{-3} (1.81×10^2)
	BP4	0.11×10^0 (0.11×10^3)	0.21×10^0 (0.21×10^4)	1.47×10^{-2} (1.47×10^3)

TABLE III. The total cross sections times the branching ratio ($\sigma \times \text{BR}$) and the expected number of signal events for the $N_R N_R H_{\text{SM}} (\rightarrow b\bar{b})$. We consider three representative center-of-mass energies of 3, 10 and 30 TeV and we show the results for the benchmark points defined in table II.

between physical observables – production cross sections, relic density and spin-independent cross sections – and model parameters as follows:

$$\begin{aligned}
\sigma_{\mu\mu \rightarrow N_R N_R H_{\text{SM}}} &\propto \lambda_3^2 \times Y_\mu^4 \times \mathcal{F}(s, M_{H^\pm}^2, M_{N_R}^2), \\
\Omega_{N_R} h^2 &\propto Y_\mu^{-4} \times \mathcal{G}(M_{H^\pm}^2, M_{N_R}^2), \\
\sigma_{\text{SI}} &\propto \lambda_3^2 \times Y_\mu^4 \times \mathcal{H}(M_{H^\pm}^2, M_{N_R}^2),
\end{aligned} \tag{7}$$

where \mathcal{F} , \mathcal{G} and \mathcal{H} are functions of $M_{N_R}^2$ and $M_{H^\pm}^2$. Therefore, it is clear that the physical observables exhibit simple scaling properties when changing from one choice of the parameters Y_μ and λ_3 to another choice. We therefore perform the following scan over the mass of the DM particle of the model

$$50 \leq M_{N_R} \leq \frac{1}{2} \left(\sqrt{s} - M_{H_{\text{SM}}} \right), \tag{8}$$

for $\Delta = 200$ GeV where $\Delta = M_{H^\pm} - M_{N_R}$. We furthermore fix $Y_\mu = 2 = \lambda_3^2$.

III. TECHNICAL SETUP

A. Signal and backgrounds

In this work, we investigate the potential discovery of dark matter at muon colliders using the mono-Higgs channel: $N_R N_R H_{\text{SM}} (\rightarrow b\bar{b})$. Our analysis focuses on collision energy $\sqrt{s} = 3$ TeV and an integrated luminosity of 1 ab^{-1} . The $N_R N_R H_{\text{SM}} (\rightarrow b\bar{b})$ process leads to a final state comprising of missing energy and at least two b -tagged jets (in the resolved case) or at least one large- R jet (in the boosted regime). The parton-level Feynman diagrams for the signal and the backgrounds are depicted in figures 1 and 2. The signal cross section receives two contributions, both occurring in t - and u -channels. The first contribution occurs through the double exchange of charged singlet scalar (1-a) while the second contribution occurs through the exchange of a muon in the t -channel (1-b). The second contribution is negligible since it is suppressed by the smallness of the Higgs-muon Yukawa coupling. The backgrounds can be split in two categories depending on their exact signature at the parton level:

- Irreducible backgrounds: This category of background involves either the production of the SM Higgs boson in association with two SM neutrinos or the production of two gauge bosons ($ZZ/WZ/WW$) where one gauge boson decays hadronically while the other decays invisibly (in the case of the Z -boson) or leptonically (in the case of W -boson) with one charged lepton escapes the detection. Note that the diboson production can be significantly reduced by requirements on the invariant of the hadronically decaying gauge boson to be off their on-shell mass window.

² Note that the choice of the other couplings Y_e and Y_τ does not affect the results of our analysis.

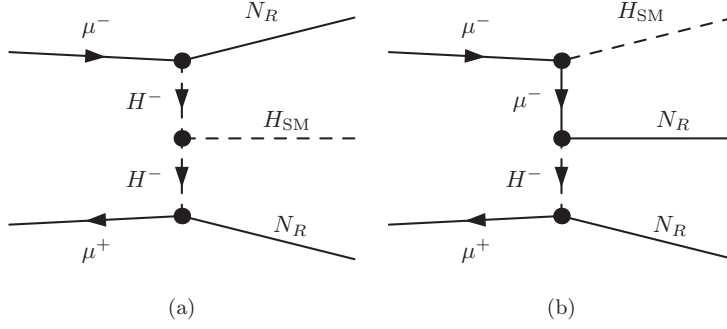


FIG. 1. Example of Feynman diagram for the signal process $\mu\mu \rightarrow N_R N_R H_{SM}$.

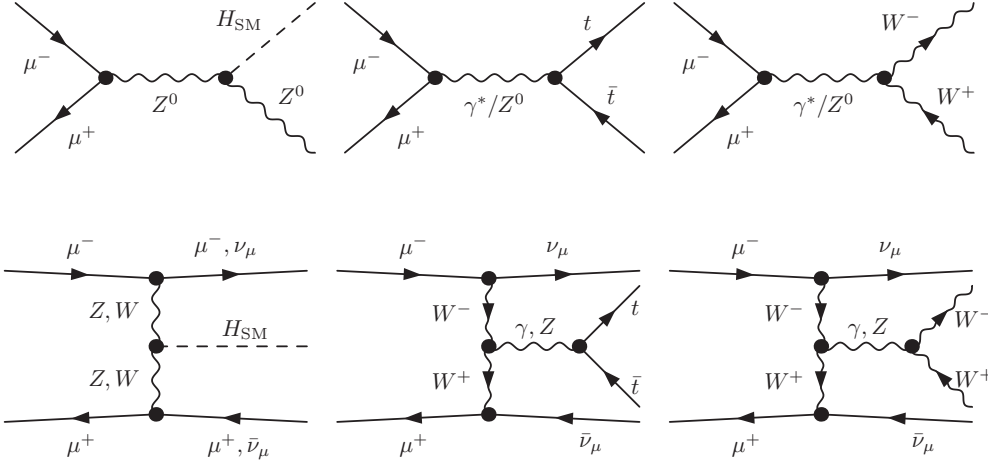


FIG. 2. Example of Feynman diagrams for the background processes contributing to the $b\bar{b} + E_T^{\text{miss}}$ final state. Here we show the muon-annihilation channels (upper panel) and VBF channels (lower panel).

- Reducible backgrounds: This category contains the production of $t\bar{t}$ and $t\bar{t} + W/Z$ or the production through neutral current VBF (i.e. involving two charged leptons). We note that this category can be significantly reduced by several requirements on the number of hard charged leptons, or requirements on the invariant mass of the $b\bar{b}$ system that will form a Higgs *candidate*.

We present the cross-section results for the signal process in Table III corresponding to the four benchmark points defined in Table II and shown in Figure 3, as a function of the DM mass (M_{N_R}). The background cross sections are shown in table IV.

B. Monte Carlo event generation

Samples for the signal and the backgrounds were generated using MADGRAPH_AMC@NLO version 3.4.1 [80] where we have used a dedicated model file in the UFO format [81] which we have produced using FEYNRULES version 2.3.0 [82]. The model file along with instructions on how to use it can be found in this [link](#). For the generation of both the signal and the background events, we have imposed some generator-level cuts:

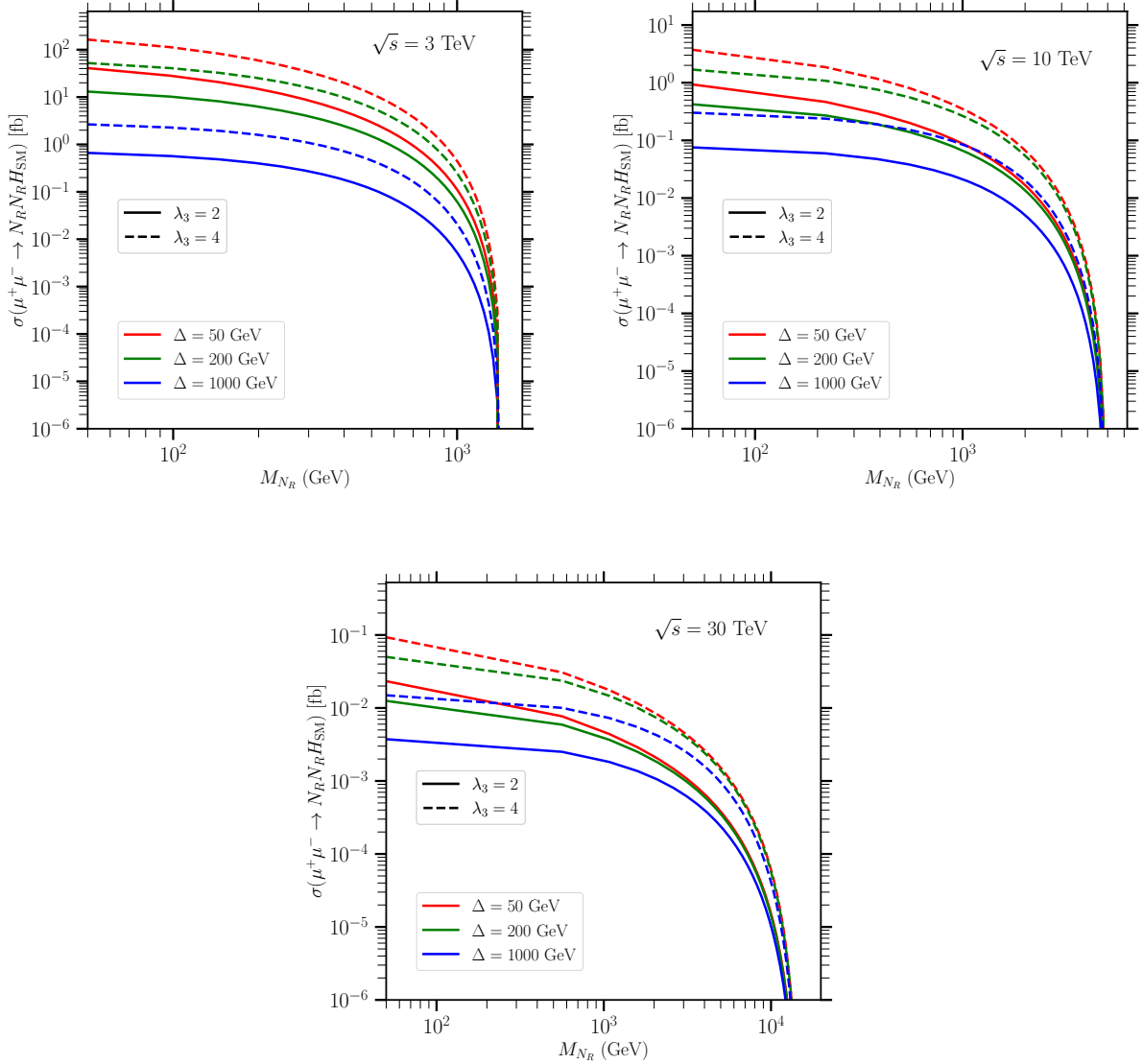


FIG. 3. The cross section for the production of $N_R N_R H_{SM}$ as a function of M_{N_R} for $\sqrt{s} = 3$ TeV (left upper panel), $\sqrt{s} = 10$ TeV (right upper panel) and $\sqrt{s} = 30$ TeV (lower panel). Here we show the results for $\lambda_3 = 2$ (solid lines) and $\lambda_3 = 4$ (dashed lines) for $\Delta = 50$ GeV (red), $\Delta = 200$ GeV (green) and $\Delta = 1000$ GeV (blue). All the calculations were done for $Y_\mu = 2$.

$$\begin{aligned}
 p_T^\ell &> 7 \text{ GeV} & \text{and} & & |\eta_\ell| < 7 \\
 p_T^j &> 10 \text{ GeV} & \text{and} & & |\eta_j| < 6.
 \end{aligned}$$

Background processes, on the other hand, receive sizeable contributions from the VBF channels, *i.e.* $VV \rightarrow X$. The computation of the rates of these processes can be done by either considering the VBF/VBS of two gauge bosons through $\mu^+ \mu^-$ process following the lines of Ref. [23] or considering that electroweak gauge bosons form partons within muons with some parton distribution functions (PDFs) within the muons [24]. Given that there is no validated treatment of initial state gauge boson PDFs for parton showers, we use the first approach in our simulation of the VBF processes in the SM. For example, to simulate $\mu^+ \mu^- \rightarrow W^* W^* \rightarrow t\bar{t} + X$, we use the following syntax in MADGRAPH5_AMC@NLO:

Center-of-mass energy	3 TeV	10 TeV	30 TeV
<i>Cross section (fb)</i>			
$\mu\mu \rightarrow H_{\text{SM}}Z$	1.37×10^0	0.12×10^0	1.37×10^{-2}
$\mu\mu \rightarrow WW$	4.67×10^2	5.89×10^1	8.26×10^0
$\mu\mu \rightarrow ZZ$	2.61×10^1	3.28×10^0	4.60×10^{-1}
$\mu\mu \rightarrow t\bar{t}$	1.91×10^1	1.72×10^0	1.92×10^{-1}
$VV \rightarrow HZ$	9.87×10^0	3.53×10^1	7.59×10^1
$VV \rightarrow H_{\text{SM}}$	4.98×10^2	8.45×10^2	1.17×10^3
$VV \rightarrow WZ$	3.98×10^1	3.19×10^1	1.26×10^1
$VV \rightarrow WW$	1.51×10^2	4.30×10^2	8.58×10^2
$VV \rightarrow ZZ$	5.66×10^1	2.03×10^2	4.30×10^2
$VV \rightarrow t\bar{t}$	5.22×10^0	1.71×10^1	3.14×10^1
$VV \rightarrow t\bar{t}W$	5.67×10^{-2}	1.05×10^{-1}	6.97×10^{-2}
$VV \rightarrow t\bar{t}Z$	1.10×10^{-1}	9.01×10^{-1}	2.77×10^0

TABLE IV. Parton-level cross sections for the background processes that we are taken into account in this study.

```

> import model sm
> generate mu+ e- > t t~ vm~ ve
> add process mu+ e- > t t~ mu+ e-
> output MyOutput

```

This syntax is necessary to isolate VBF contributions from the corrections of initial-state radiation (ISR) or final-state radiation (FSR) to s -channel contributions. Note that the syntax above corresponds to μ^+e^- scatterings and similar results can be found if we consider the complex conjugate of it, *i.e.* μ^-e^+ scatterings. In our calculations, we have considered both neutral-current as well as charged-current contributions to the VBF processes. For example, $VV \rightarrow t\bar{t}$ in table IV includes both contributions from $\mu^+e^- \rightarrow t\bar{t}\bar{\nu}_\mu\nu_e$ and $\mu^+e^- \rightarrow t\bar{t}\mu^+e^-$. We have checked that our calculations of the background cross sections yield excellent agreement with the results of ref. [23]. As for the signal processes, we found that there is no contribution to the production of the N_R through VBF. This can be understood since the N_R particles are $SU(2)_L \otimes U(1)_Y$ singlets and therefore do not couple directly to γ/Z or W gauge bosons. For each benchmark point in the signal and for all the backgrounds we have generated about $9 \times 10^5 - 3 \times 10^6$ parton-level events. The produced events are passed to PYTHIA version 8307 [83] to add resonance decays, parton showering and hadronisation.

C. Object definitions

In this section, we discuss the object definitions at the reconstruction level that we have used in our analysis. In this work, we define charged leptons (electrons or muons), hadronically decaying tau leptons (τ_h), small- R jets, large- R jets and missing transverse momentum. The details are shown below:

- **Electron candidates:** Are required to have $p_T^e > 7$ GeV and $|\eta| < 6$.
- **Muon candidates:** Muon candidates are required to have $p_T > 7$ GeV and $|\eta| < 6$.
- **Hadronically-decaying tau leptons:** Those are reconstructed from their one-, two- and three-prong decays and are required to have $p_T > 15$ GeV and $|\eta_\tau| < 2.5$. We assume a τ -tagging efficiency of 60% (70%) if the number of associated tracks is ≥ 2 (1).
- **Small- R Jets:** Candidate jets are reconstructed with the anti- k_t algorithm with a radius parameter $R = 0.4$ which are referred to as “small- R jets” [84]. These jets are further required to have $p_T > 25$ GeV and $|\eta_j| < 6$. We use a ghost-based approach to tag “small- R jets” as b -jets where we assume a 70% b -tagging efficiency and a p_T -dependent mistagging efficiency of light and charm jets as b -jets, *i.e.*

$$\begin{aligned}
\mathcal{E}_{c|b} &= 0.20 \tanh(0.02p_T) \frac{1}{1 + 0.0035p_T} \\
\mathcal{E}_{j|b} &= 0.002 + 7.3 \times 10^{-6} p_T.
\end{aligned}
\tag{9}$$

With these parameterisations one gets $\mathcal{E}_{j|b} = 0.002$ (0.009) and $\mathcal{E}_{c|b} = 0.085$ (0.045) for $p_T = 25$ (1000) GeV. b -tagged jets are required to have $p_T > 25$ GeV and $|\eta_b| < 2.5$.

- **Large- R Jets:** In our analysis, the SM Higgs boson can be produced with very high transverse momentum. In such cases, the hadronic decay products of the SM Higgs boson can not be resolved into two isolated jets and therefore clustering based on small- R jet radius will have very small efficiencies. Therefore, we also utilize large- R jets in our analysis. A large radius parameter is chosen in order for a single large- R jet to capture all the constituents that are produced in the decay of a boosted Higgs boson. We perform two independent clustering algorithms along the same lines of the ATLAS [78] and CMS [79] analyses. First, we cluster jets using the anti- k_t clustering algorithm with a jet radius of $R = 1$ [84] and these jets will be labeled as AK10 jets. Furthermore, we apply a trimming algorithm to remove any soft radiation [85]. For this purpose we use the k_t algorithm [86] where we remove any subjet of radius $R = 0.2$ that carries less than 5% of the total AK10 jet energy. An independent clustering algorithm will be used in our analysis where we cluster the jets using the Cambridge-Aachen algorithm and a jet radius of $R = 1.5$ [87] which will be denoted as CA15 jets. In this case, the soft-drop jet grooming algorithm [88] is employed to cut soft and wide-angle radiation from the CA15 jets where we use $\beta = 1$ and $z_{\text{cut}} = 0.1$. For the training of the signal and the backgrounds and in order to optimise the sensitivity of the analysis, we use the ratios of the energy correlation functions constructed from the output of the CA15 jets. In this analysis, we construct two variables N_2 and M_2 which were found to be very powerful in discriminating two-prong boosted objects from QCD jets or three-prong boosted jets [89]. They are defined as

$$M_2^{(\beta)} = \frac{1e_3^{(\beta)}}{1e_2^{(\beta)}}, \quad N_2^{(\beta)} = \frac{2e_3^{(\beta)}}{(1e_2^{(\beta)})^2}, \quad (10)$$

where ${}_k e_i^{(\beta)}$ are the generalized i -point energy correlation function for the k pair-wise angles that enters their products and β is a parameter that controls the overall angular scaling of these operators. In this analysis, we choose β to be equal to 1. All the large- R jets are required to have $p_T > 200$ GeV and $|\eta| < 2.5$.

- **Missing Transverse Energy:** The missing transverse momentum $\mathbf{p}_T^{\text{miss}}$ (with magnitude E_T^{miss}) is the negative vector sum of the p_T of all selected and calibrated objects in the event, including a term to account for energy from soft particles in the event which are not associated with any of the selected objects.

We further impose isolation requirements on charged leptons. A lepton isolation criterion is defined by imposing a cut on the following quantity

$$I_R \equiv \sum_{i \in \text{tracks}} p_T^i,$$

where the sum includes all tracks (excluding the lepton candidate itself) within the cone defined by $\Delta R < R_{\text{cut}}$ about the direction of the charged lepton. The value of R_{cut} is the smaller of r_{min} and $10 \text{ GeV}/p_T^\ell$, where r_{min} is set to 0.3 for both the electron and the muon candidates, and p_T^ℓ is the lepton transverse momentum. All the charged lepton candidates must satisfy

$$I_R/p_T^\ell < 0.3,$$

which defines a loose-isolation criterion. Overlap removals are used to remove leptons or jets if they are within some defined ΔR of a given object. Electron (muon) candidates that lie within $\Delta R = 0.2$ (0.4) of a jet candidate. Jets are also required to have $\Delta R = 0.4$ of other leptons or jets in the event.

Fast detector simulation is performed using the SFS module [90] in MADANALYSIS 5 [91–96]. The calculation of the jet observables including the clustering of large- R jets and the removal of the soft radiation is done with the help of customised C++ analysis within the `Substructure` module [97]. All the jets were clustered using FASTJET version 3.4.0 [98]. The momentum smearing and identification efficiencies for electrons are implemented from the detector design of FCC-hh that is shipped in DELPHES 3.4.0 [99] (can be found in https://github.com/delphes/delphes/blob/master/cards/delphes_card_MuonColliderDet.tcl). For muons smearing and identification efficiencies we use the results of Ref. [100].

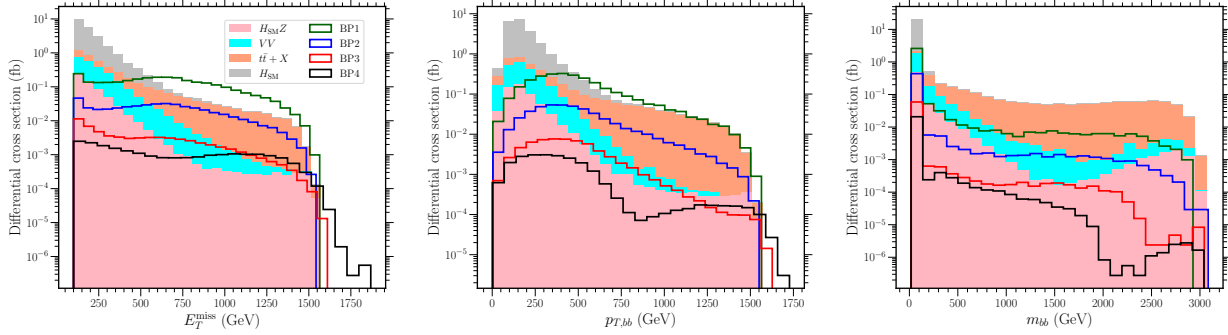


FIG. 4. Differential cross section per bin for the four benchmark points defined in Table II and the background processes shown as stacked histograms in the resolved regime. From the left to the right, we show the missing transverse energy, the transverse momentum of the Higgs candidate and, the invariant mass of the Higgs candidate. More details can be found in the text.

IV. CUT-BASED ANALYSIS

In this section we discuss the basic approach for the signal-to-background analysis which consists of performing basic event selection on both the signal and the background processes. In this analysis, we follow the analysis strategies of the recent ATLAS [78] and CMS [79] searches of DM produced in association with a Higgs boson and decaying to bottom quarks.

A. Resolved regime

For the resolved regime, we assume that the Higgs boson candidate is reconstructed from two small- R well-separated b -tagged jets. The key distributions for the signal-to-background optimisations are shown in Fig. 4. First, we require that the missing transverse energy is larger than 100 GeV. Electrons and muons that pass the loose isolation criteria defined in the previous section are vetoed. This criterion reduces the VBF processes that occur through neutral current interactions, *i.e.* $Z^*Z^* \rightarrow X$. Events that contain at least one hadronically-decaying τ -lepton satisfying $p_T^\tau > 15$ GeV and $|\eta^\tau| < 6$ are vetoed. We do not require the existence of any photon with $p_T > 10$ GeV and $|\eta| < 6$. We furthermore require that the events contain at least three small- R untagged jets that satisfy $p_T > 25$ GeV and $|\eta| < 6$ where at least two of them are b -tagged with $|\eta^b| < 2.5$. To reduce backgrounds where E_T^{miss} arose from mismeasurement of the jet p_T or from leptonic decays of heavy flavours, we require that the minimum $\Delta\phi$ defined by

$$\Delta\phi_{\min} \equiv \min \left\{ \Delta\phi(\mathbf{p}_{\text{miss}}, \mathbf{j}_1), \Delta\phi(\mathbf{p}_{\text{miss}}, \mathbf{j}_2), \Delta\phi(\mathbf{p}_{\text{miss}}, \mathbf{j}_3) \right\},$$

to be larger than 20° . Here, $\Delta\phi(x, y) \equiv |\phi_x - \phi_y|$ and $\mathbf{j}_{1,2,3}$ are the momenta of the three leading jets in the event. The Higgs boson candidate is reconstructed from the momenta of the two leading b -jets. Therefore, we require that all the events have exactly two b -jets. To be sure that we restrict the analysis in the resolved regime, we further require that $E_T^{\text{miss}} \in]300, 1000]$ GeV. Note that this requirement is slightly different from the ATLAS definition of the resolved region [78]. Higgs boson candidates are required to have a transverse momentum that is larger than 300 GeV. To ensure that reconstructed Higgs boson candidate and the missing transverse momentum (\mathbf{p}_{miss}) are back-to-back, we require that $\Delta\phi(\mathbf{p}_{\text{miss}}, \mathbf{p}_H) > 2\pi/3$. Backgrounds where E_T^{miss} originates from leptonically-decaying W -boson have the particular property that the transverse mass formed by E_T^{miss} and either the leading or the subleading b -jets to be bounded by the top quark mass from above. These two variables are defined as

$$\begin{aligned} m_T^{\min} &\equiv \sqrt{2 p_T^{\text{lead}} E_T^{\text{miss}} (1 - \cos \Delta\phi(\mathbf{b}_{\text{lead}}, \mathbf{p}_{\text{miss}}))}, \\ m_T^{\max} &\equiv \sqrt{2 p_T^{\text{lead}} E_T^{\text{miss}} (1 - \cos \Delta\phi(\mathbf{b}_{\text{lead}}, \mathbf{p}_{\text{miss}}))}, \end{aligned} \quad (11)$$

	$VV + X$		$t\bar{t} + X$		$H + X$		BP1	
	Events	ϵ	Events	ϵ	Events	ϵ	Events	ϵ
Initial	7.4×10^5	-	24367.3	-	5.1×10^5	-	20500.0	-
$E_T^{\text{miss}} > 100$ GeV	$2.5 \times 10^5 \pm 90.6$	0.332	17285.9 ± 8.3	0.709	$1.6 \times 10^5 \pm 73.7$	0.315	15153.9 ± 9.2	0.739
Lepton veto	$1.6 \times 10^5 \pm 67.0$	0.670	13647.4 ± 8.0	0.790	$1.5 \times 10^5 \pm 72.5$	0.961	15108.2 ± 9.3	0.997
τ veto	$1.5 \times 10^5 \pm 60.1$	0.898	12061.3 ± 7.6	0.884	$1.5 \times 10^5 \pm 72.1$	0.966	14880.0 ± 9.3	0.985
Photon veto	$1.4 \times 10^5 \pm 56.2$	0.937	10998.0 ± 7.2	0.912	$1.5 \times 10^5 \pm 72.0$	0.990	14622.4 ± 9.4	0.983
≥ 2 small-R jets	$1.0 \times 10^5 \pm 41.6$	0.727	8967.4 ± 6.1	0.815	82718.7 ± 46.7	0.561	10729.8 ± 8.9	0.734
≥ 2 b -jets	1904.6 ± 0.6	0.019	1920.4 ± 1.6	0.214	19203.6 ± 12.8	0.232	929.2 ± 1.1	0.087
$\Delta\phi > 0.35$	1732.2 ± 0.6	0.909	1190.6 ± 0.9	0.620	19155.7 ± 13.1	0.998	769.3 ± 0.9	0.828
$N_b = 2$	1617.7 ± 0.5	0.934	1133.2 ± 0.9	0.952	19064.6 ± 13.4	0.995	764.8 ± 0.9	0.994
$E_T^{\text{miss}} \in]300, 1000]$ GeV	402.3 ± 0.1	0.249	432.4 ± 0.4	0.382	2195.4 ± 1.3	0.115	549.6 ± 0.6	0.719
$p_T^{b\bar{b}} > 300$ GeV	230.7 ± 0.1	0.574	319.5 ± 0.3	0.739	1942.0 ± 1.3	0.885	446.3 ± 0.5	0.812
$\Delta\phi(\vec{p}_{\text{miss}}, \vec{p}_H) > 2\pi/3$	224.2 ± 0.1	0.972	306.4 ± 0.3	0.959	1941.7 ± 1.3	1.000	317.7 ± 0.4	0.712
$m_{T,b}^{\text{min}} > 170$ GeV	208.5 ± 0.1	0.930	129.5 ± 0.1	0.422	1928.3 ± 1.4	0.993	314.0 ± 0.4	0.988
$m_{T,b}^{\text{max}} > 200$ GeV	208.0 ± 0.1	0.998	129.4 ± 0.1	1.000	1927.6 ± 1.4	1.000	313.6 ± 0.4	0.999
$N_{\text{jets}} < 3$	183.3 ± 0.1	0.882	81.7 ± 0.1	0.632	1921.4 ± 1.4	0.997	312.5 ± 0.4	0.996
$m_{b\bar{b}} \in]80, 160[$ GeV	7.5 ± 0.0	0.041	3.6 ± 0.0	0.045	1520.7 ± 1.2	0.791	216.2 ± 0.3	0.692

TABLE V. The cutflow table for the event selection used in the resolved region for the backgrounds and an example of the signal event (BP1). For each entry we show the number of events after each selection step along with the statistical uncertainty. We also show the efficiency after each selection as defined in eq. 12.

with p_T^{lead} and p_T^{sublead} refer to the p_T of the leading and the subleading b -jets respectively and $\Delta\phi(x, y) \equiv |\phi_a - \phi_b|$. We require that $m_T^{\text{min}} > 170$ GeV and $m_T^{\text{max}} > 200$ GeV. The total number of jets that includes both tagged and untagged jets is required to be less than 3. The effect of this cut is however very minor on all the processes. Finally, we require that the invariant of the Higgs candidate to satisfy

$$80 \text{ GeV} < m_{b\bar{b}} < 160 \text{ GeV}.$$

In Table V we show the cutflow table in the resolved analysis for both the backgrounds ($VV + X$, $t\bar{t} + X$ and $H + X$) and the signal. For the signal we show only the example of BP1. In each selection we calculate the MC uncertainty that arise from the statistical limitation and the acceptance times the efficiency defined as

$$\epsilon \equiv \frac{N_i}{N_{i-1}}, \quad (12)$$

where N_i and N_{i-1} correspond to the number of events that survive the selection i and $i - 1$ respectively. We can see that the requirement on having at least two b -tagged jets kills about 82% of the signal events which is not in agreement with the naive expectation of $\epsilon \propto \epsilon_b^2 \approx 49\%$ (ϵ_b is the b -tagging efficiency)³. After all the selections we get an accumulated efficiency of about 0.9%-1.2% for the signal which is slightly dependent on the DM mass assumption while for the backgrounds we get an overall efficiency of 0.1%. We also calculate the significance using Asimov formula [102]. The results of this calculation for the four benchmark points are shown in Table VI.

³ This is due to the fact that the Higgs boson produced in association with DM particles is highly boosted and that its decay products can not be resolved. As an example, for a Higgs boson decaying into $b\bar{b}$, the $\Delta R_{b\bar{b}}$ separation is roughly given by [101]

$$\Delta R_{b\bar{b}} \propto \frac{M_{H_{\text{SM}}}}{p_{T,H}} \times (z_b z_{\bar{b}})^{-1/2}$$

where z_b and $z_{\bar{b}}$ are the momentum fractions for the bottom and the anti-bottom quarks. For the SM Higgs boson with transverse momentum in the range [500, 1000] GeV decaying democratically, *i.e.* $z_b = z_{\bar{b}} = 1/2$ we have $\Delta R_{b\bar{b}} \approx 0.06$ -0.1.

Benchmark point	BP1	BP2	BP3	BP4
\mathcal{S}	5.40	1.61	0.14	2.62×10^{-2}

TABLE VI. Signal significance for the four benchmark points in the resolved regime.

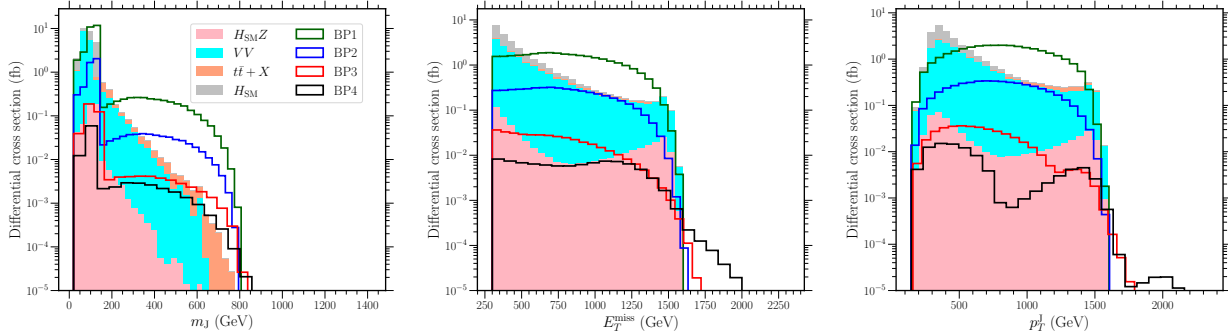


FIG. 5. Differential cross section per bin for the four benchmark points defined in Table II and the background processes shown as stacked histograms in the merged regime for the AK10 jet category. We show the invariant mass of the leading trimmed jet m_J (left panel), the missing transverse energy E_T^{miss} (middle panel) and the transverse momentum of the leading trimmed jet p_T^J (right panel).

	$VV + X$		$t\bar{t} + X$		$H + X$		BP1	
	Events	ϵ	Events	ϵ	Events	ϵ	Events	ϵ
Initial	7.4×10^5	-	24367.3	-	5.1×10^5	-	20500.0	-
Lepton Veto	$4.8 \times 10^5 \pm 157.6$	0.652	18123.7 ± 7.9	0.744	$4.7 \times 10^5 \pm 91.4$	0.923	20371.8 ± 1.9	0.994
τ Veto	$4.6 \times 10^5 \pm 156.5$	0.956	16321.9 ± 8.0	0.901	$4.5 \times 10^5 \pm 109.2$	0.955	20029.1 ± 3.6	0.983
$E_T^{\text{miss}} > 300$ GeV	39334.6 ± 18.6	0.085	7076.6 ± 6.1	0.434	12253.7 ± 3.1	0.027	12014.1 ± 9.2	0.600
$N_{\text{AK10 jets}} > 0$	37221.1 ± 17.8	0.946	7052.4 ± 6.0	0.997	10898.5 ± 2.6	0.889	10923.8 ± 8.9	0.909
$M_J \in]70, 180[$ GeV	31233.4 ± 15.0	0.839	4975.3 ± 4.5	0.705	9202.1 ± 2.2	0.844	8377.4 ± 7.7	0.767

TABLE VII. Same as in Table V but for the boosted regime with AK10 jets.

B. Merged regime

As was shown in the previous subsection, the SM Higgs boson produced in the mono-Higgs channel leads to unresolved hadronic decay products. Therefore, one expects that the boosted (or merged) selection would have a higher sensitivity reach. In this subsection we perform a cut-based analysis of the mono-Higgs channel using jet substructure techniques. We perform two independent search strategies inspired by the ATLAS [78] and CMS [79] boosted analyses. Therefore, we employ two different jet clustering algorithms although using the same selection criteria (see section III C for more details):

- First analysis category: We cluster jets using the anti- k_t algorithm and a jet radius of $R = 1$ (denoted by AK10). We use a trimming algorithm that is based on the k_t algorithm and removing subjets of radius $R = 0.2$ that carry less than 5% of the total AK10 jet energy.
- Second analysis category: We cluster jets using the Cambridge-Aachen algorithm and a jet radius of $R = 1.5$ (denoted by CA15). We use a soft drop algorithm to remove soft and a wide-angle radiation.

The differential distributions for the key observables are shown in Fig. 5 (for the selection based on AK10 jets) and in Fig. 6 (for the selection based on the CA15 jets). We require that events do not contain any isolated lepton (electron or muon) with $p_T > 7$ GeV and $|\eta| < 6$. Furthermore, we veto events that contain

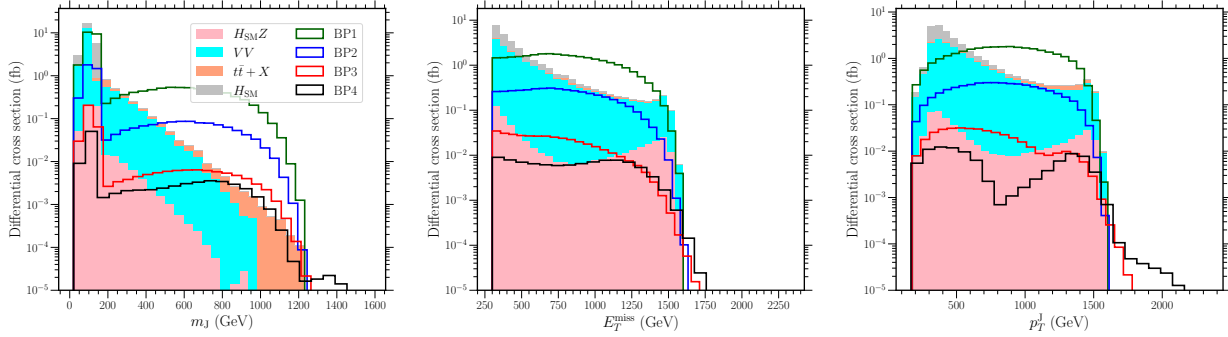


FIG. 6. Differential cross section per bin for the four benchmark points defined in Table II and the background processes shown as stacked histograms in the merged regime for the AK10 jet category. We show the invariant mass of the leading trimmed jet m_J (left panel), the missing transverse energy E_T^{miss} (middle panel) and the transverse momentum of the leading trimmed jet p_T^J (right panel).

	$VV + X$		$t\bar{t} + X$		$H + X$		BP1	
	Events	ϵ	Events	ϵ	Events	ϵ	Events	ϵ
Initial	7.4×10^5	-	24367.3	-	5.1×10^5	-	20500.0	-
Lepton Veto	$4.8 \times 10^5 \pm 157.6$	0.652	18123.7 ± 7.9	0.744	$4.7 \times 10^5 \pm 91.4$	0.923	20371.8 ± 1.9	0.994
τ Veto	$4.6 \times 10^5 \pm 156.5$	0.956	16321.9 ± 8.0	0.901	$4.5 \times 10^5 \pm 109.2$	0.955	20029.1 ± 3.6	0.983
$E_T^{\text{miss}} > 300$ GeV	39334.6 ± 18.6	0.085	7076.6 ± 6.1	0.434	12253.7 ± 3.1	0.027	12014.1 ± 9.2	0.600
$N_{\text{CA15 jets}} > 0$	39166.6 ± 18.6	0.996	7075.5 ± 6.1	1.000	12182.3 ± 3.0	0.994	12014.1 ± 9.2	1.000
$N_{\text{SD jets}} > 0$	37419.0 ± 17.9	0.955	7060.5 ± 6.0	0.998	11083.4 ± 2.7	0.910	11118.7 ± 9.0	0.925
$M_{\text{SD}} \in]70, 180[$ GeV	31615.2 ± 15.3	0.845	4233.1 ± 3.9	0.600	9625.0 ± 2.3	0.868	6978.8 ± 6.8	0.628

TABLE VIII. Same as in Table V but for the boosted regime with CA15 jets.

Benchmark point		BP1	BP2	BP3	BP4
\mathcal{S}	AK10 jets	38.18	10.91	0.84	0.17
	CA15 jets	31.93	9.02	0.74	0.15
p	AK10 jets	0.15	4.91×10^{-2}	3.95×10^{-3}	8.23×10^{-4}
	CA15 jets	0.13	4.08×10^{-2}	3.46×10^{-3}	7.06×10^{-4}

TABLE IX. Signal significance (\mathcal{S}) and purity (p) for the four benchmark points in the boosted regime for the AK10 jets (first rows) and CA15 jets (second rows).

one hadronically decaying τ -lepton having $p_T > 15$ GeV and $|\eta| < 2.5$. We then require that the missing transverse energy satisfies $E_T^{\text{miss}} > 300$ GeV. Signal-like events are required to have at least one AK10 jet with $p_T > 150$ GeV and $|\eta| < 2.5$ or at least one CA15 jet with $p_T > 150$ GeV and $|\eta| < 2.5$. The fat jets that pass these requirements are either trimmed (for AK10 jets) or soft-dropped (for CA15 jets). Therefore one requires that events contain at least one trimmed jet for the ATLAS-like analysis or at least one soft-dropped jet for the CMS-like analysis. The leading trimmed or soft-dropped jet is required to have $M > 20$ GeV. Finally we require that the leading fat jet to have an invariant mass satisfying $70 \text{ GeV} < M < 180 \text{ GeV}$. The last cut defines our signal region. The cutflow tables are shown in Tables VII and VIII. The acceptance times the efficiency for the signal varies in the range 34%–41% for the AK10 jets and in the range of 29%–39% for

the CA15 jets. Finally, we calculate both the significance (defined in eq. 14) and the purity⁴ of the signal for the four benchmark points and we display the results in Table IX. We find that the signal significance for the merged regime is a factor of 6–10 larger than that in the case of the resolved regime.

V. OPTIMISATION USING BOOSTED-DECISION TREES

A. General setup

An improvement of the previous results can be achieved by using Machine Learning (ML) algorithms, such as decision trees (BDTs). The BDT training is performed using the four benchmark points described in Table II which are merged in one signal sample and for the background sample we merge all the SM background processes. All the processes are weighted by their generator-level cross sections since each process, for both the signal and the background, has a different cross section. Furthermore, in the case where the MC samples for the signal contain more events than the background samples, we reweight the signal and background samples using weight computed via the `compute_sample_weight` as implemented in SCIKIT-LEARN [103]. The BDT algorithm was implemented using XGBOOST classifier [104]. The model has been trained using a feature set consisting of the following variables:

- **Resolved regime:**

$$\{E_T^{\text{miss}}, \phi_{\text{miss}}, p_{T,b}^i, \phi_b^i, \eta_b^i, E_b^i, p_T^{bb}, \phi_{bb}, \eta_{bb}, E_{bb}, m_{bb}, \Delta\phi(\vec{b}_1, \vec{p}_{\text{miss}}), \Delta\phi(\vec{b}_2, \vec{p}_{\text{miss}}), m_T^{\text{min}}, m_T^{\text{max}}\}$$

- **Boosted regime with AK10 jets:**

$$\{E_T^{\text{miss}}, \phi_{\text{miss}}, p_T^J, \eta_J, \phi_J, E_J, m_J, \Delta\phi(\vec{J}, \vec{p}_{\text{miss}}), m_T(\text{J}, E_T^{\text{miss}})\}$$

- **Boosted regime with CA15 jets:**

$$\{E_T^{\text{miss}}, \phi_{\text{miss}}, p_T^J, \eta_J, \phi_J, E_J, m_J, \Delta\phi(\vec{J}, \vec{p}_{\text{miss}}), m_T(\text{J}, E_T^{\text{miss}}), M_2^{(\beta)}, N_2^{(\beta)}\}$$

where m_T is defined as

$$m_T(\text{J}, E_T^{\text{miss}}) \equiv \sqrt{2 p_T^J E_T^{\text{miss}} (1 - \cos \Delta\phi(\vec{J}, \vec{p}_{\text{miss}}))} \quad (13)$$

We briefly describe the event preselection criteria applied in our analysis. For the resolved regime, we follow the same selection steps as in the cut-based analysis but halt the selection process once we achieve the requirement of having exactly two b -tagged jets. No further cuts on the magnitude of the missing energy are applied, except the basic requirement of $E_T^{\text{miss}} > 100$ GeV. For the boosted regime, we do not impose requirements on the invariant mass of the trimmed leading AK10 jet or the soft-dropped CA15 jets. With these requirements, we ensure enough statistics for the training. We found that some of the variables used in this study are highly correlated to m_{bb} (in the resolved regime) and to m_J (in the boosted regime). To reduce these correlations of these variables we scale p_T^b and p_T^{bb} by m_{bb} and scale p_T^J by m_J . Note that we do not apply a `StandardScaler()` function which removes the mean and reduces the variance to unity but instead, we apply a customised scaling whose aim is only for reducing the correlations. A careful inspection of the input variables through the calculation of the feature importance is very crucial to assess which of the variables can be the best signal-to-background discriminators. This can be seen in Fig. 7 where we show the feature importance for each of the input variables in the resolved regime (left panel), merged regime with AK10 jets (middle panel) and merged regime with CA15 jets (right panel). As expected, we can see that the missing transverse energy is the most sensitive feature for the model training. The other variables depend on the regime. For the resolved regime, the transverse momentum of the Higgs boson candidate ($p_{T,bb}$) and

⁴ The signal purity is defined as

$$p = \frac{n_s}{n_s + n_b},$$

where n_s (n_b) being the number of the signal (background) events after the full selection.

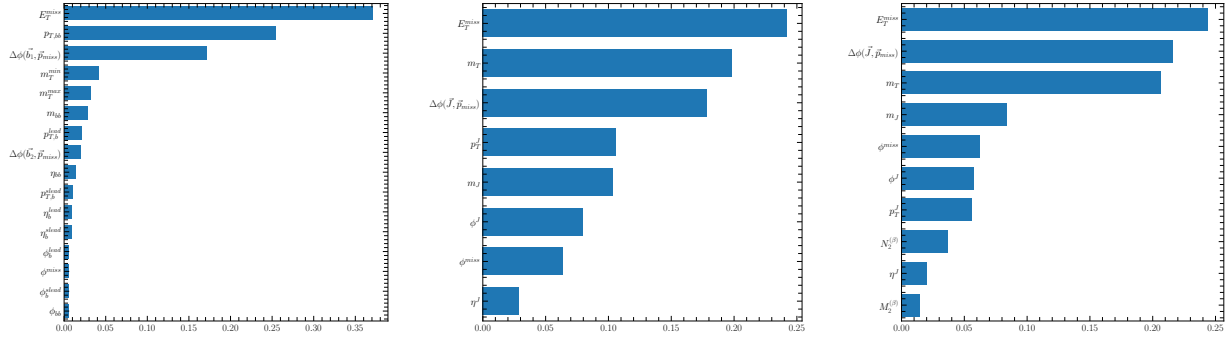


FIG. 7. Feature importance for the resolved regime (left panel), boosted regime with AK10 jets (middle panel) and boosted regime with CA15 jets (right panel).

Parameter	Purpose	Default value	This work
<code>subsample</code>	Subsample ratio of the training instances	0.5	0.8
<code>scale_pos_weight</code>	Control the balance between positive and negative weights	1	6
<code>reg_lambda</code>	L2 regularization term on the weights	0	10
<code>reg_alpha</code>	L1 regularization term on the weights	0	5
<code>n_estimators</code>	The number of runs to learn from data	—	750
<code>min_child_weight</code>	Minimum sum of instance weight (hessian) needed in a child	1	2
<code>max_depth</code>	Maximum depth of a tree	6	8
<code>learning_rate</code>	Step size shrinkage used in update to prevents overtraining	0.3	0.1
<code>colsample_bytree</code>	The subsample ratio of columns when constructing each tree	0.5	0.7
<code>tree_method</code>	The tree construction algorithm used in XGBoost	'auto'	'hist'

TABLE X. Hyperparameters of the training models used in this analysis.

the azimuthal separation between the leading b -jet and the missing momentum are very important. For the merged regime, the transverse mass m_T , the azimuthal separation between the leading fat jet and the missing momentum $-\Delta\phi(\vec{J}, \vec{p}_{\text{miss}})$, and the invariant mass of the leading fat jet (m_J) are very important features.

To avoid overtraining effects, the standard procedure is to randomly split the data into two independent datasets: a training dataset and a testing dataset. Ensuring strong alignment between the trained model and the predicted testing data serves as a good indicator of the absence of overtraining effects. However, in this study, we adopt an alternative approach. A cross-validation strategy with 5 folds is employed for the training: the data is split into 5 equal parts, a BDT model is trained on each fold and applied to the remaining 4 folds, and the final BDT score is taken to be the average of the 5 BDT model outputs. The 5 BDT models used the exact hyperparameters were optimized using the grid-search technique. The optimized hyperparameters are given in Table X. To define the final BDT score binning, the BDT score (the average of 5 BDT model outputs) is scanned for maximum significance using the Asimov formula. Each BDT bin is required to have at least one background event to ensure good statistics. The result of the scan shows that the BDT score bin $[0.99, 1]$ gives the highest significance (as expected) for the different benchmarks, thus this bin is used to define the signal region.

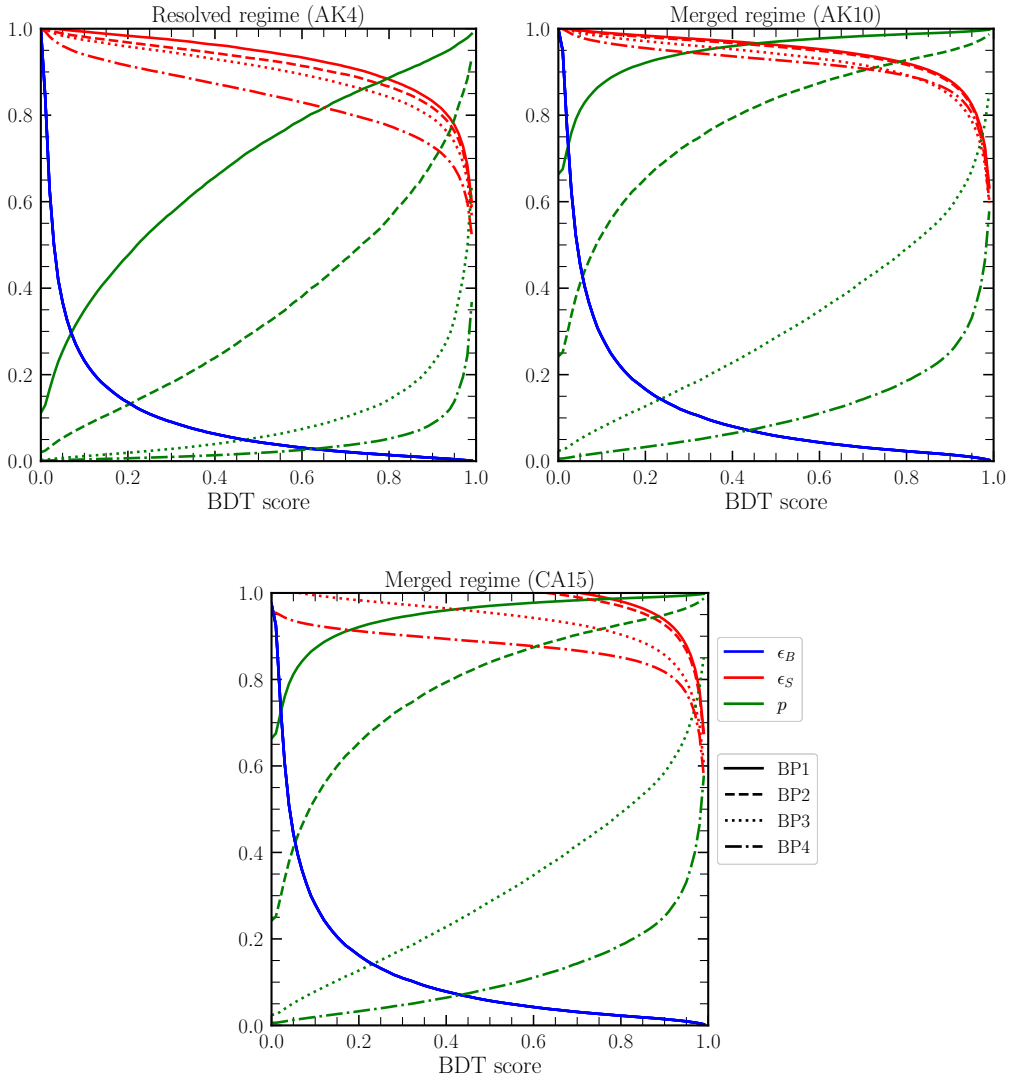


FIG. 8. The background efficiency (blue), signal efficiency (red) and signal purity (green) as a function of the cut on the BDT score. Results are shown for the resolved regime (left upper panel), the merged regime with AK10 jets (right upper panel) and the merged regime with CA15 jets (lower panels). The calculations are done for BP1 (solid), BP2 (dashed), BP3 (dotted) and BP4 (dashdotted).

B. Results

In this section we discuss the results of the BDT analysis. We first start by showing the signal purity (p), background efficiency (ϵ_B), and the signal efficiency (ϵ_S) as a function of the BDT score for the four benchmark points in figure 8. We can see that the bin with the highest BDT score (> 0.99) does not only maximise the significance but also the signal purity. The number of events for the signal is found to be quite large for most of the benchmark points with the results being more important for the merged regime than in the resolved regime. The signal purity varies in the range of 40%–99% where higher numbers are reached for the benchmark points BP1 and BP2. High values of the signal purity implies unprecedented opportunities to perform post-discovery analyses to assess the nature of DM at muon colliders. We must stress that our analysis has a very high accuracy since the area under the Receiver-Operating Characteristic (ROC) curve varies in the range of 0.95–0.97.

Benchmark point		BP1	BP2	BP3	BP4
Resolved (AK4)	$\mathcal{S}_{100 \text{ fb}^{-1}}$	33.85	9.59	1.77	0.63
	$\mathcal{S}_{1000 \text{ fb}^{-1}}$	75.69	21.45	3.97	1.42
Merged (AK10)	$\mathcal{S}_{100 \text{ fb}^{-1}}$	143.44	45.41	6.86	1.99
	$\mathcal{S}_{1000 \text{ fb}^{-1}}$	320.76	101.55	15.34	4.45
Merged (CA15)	$\mathcal{S}_{100 \text{ fb}^{-1}}$	149.20	47.83	7.66	2.60
	$\mathcal{S}_{1000 \text{ fb}^{-1}}$	333.62	106.95	17.13	5.81

TABLE XI. Signal significance (\mathcal{S}) the four benchmark points using the BDT signal region. For each entry, we show the significance for $\mathcal{L} = 100 \text{ fb}^{-1}$ and after the full run at $\mathcal{L} = 1000 \text{ fb}^{-1}$. The results are shown for the resolved regime with AK4 jets and for the two cases of the merged regime for AK10 jets and CA15 jets.

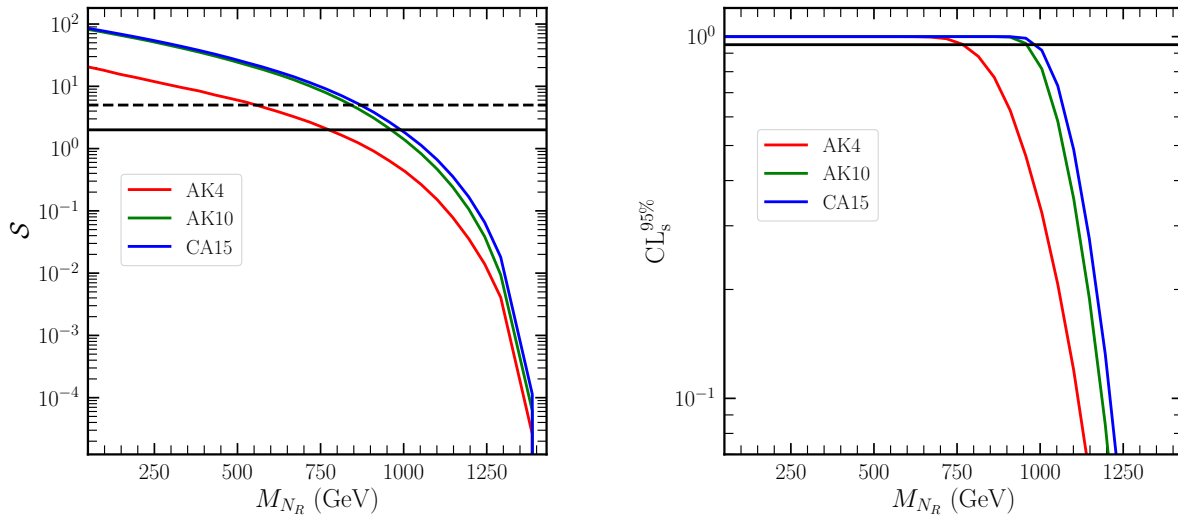


FIG. 9. Signal significance (left) and $\text{CL}_s^{95\%}$ (right) as a function of the DM mass (M_{N_R}). The results are shown for the resolved regime (red), boosted regime with AK10 jets (green) and the boosted regime with CA15 jets (blue). The black solid and dashed lines in the left panel correspond to $\mathcal{S} = 2$ and $\mathcal{S} = 5$. On the right panel, the solid black line corresponds to $\text{CL}_s = 0.95$ above which the mass value is excluded at 95% CL.

We also calculate the signal significance for the signal using Asimov formula [102]

$$\mathcal{S} \equiv \sqrt{2 \left((n_s + n_b) \log \left(1 + \frac{n_s}{n_b} \right) - n_s \right)}, \quad (14)$$

for both $\mathcal{L} = 100 \text{ fb}^{-1}$ and $\mathcal{L} = 1 \text{ ab}^{-1}$ for the BDT bin > 0.99 . The results are shown in Table XI. We can see that even for a luminosity of 100 fb^{-1} the BDT search strategy leads to quite large signal significance for BP1, BP2 and BP3 where high values are reached for the boosted regime as expected. To reach a high signal significance for BP4 (corresponding to heavy DM), the full luminosity of 1 ab^{-1} is required. We notice that very important improvements with respect to the results of the cut-based analysis are reached when comparing the results of Table XI with those shown in Tables VI and IX. The results are improved by about 8–50 depending on the benchmark point and the kinematic regime. For instance, BP4 receives the highest improvement especially for the resolved regime where \mathcal{S} increases from 2.62×10^{-2} to 1.42.

Finally, we use the trained algorithm to optimise the signal-over-background ratio for DM mass in the interval defined in equation 8. In other words, no further training has been performed at this stage. To quan-

tify the sensitivity reach of this analysis we calculate both the significance and the $\text{CL}_s^{95\%}$. The significance is calculated by assuming some uncertainties on the background yields and is defined as

$$\mathcal{S} = \sqrt{2} \left[(n_s + n_b) \log \left(\frac{(n_s + n_b)(n_b + \delta_b^2)}{n_b^2 + (n_s + n_b)\delta_b^2} \right) - \frac{n_b^2}{\delta_b^2} \log \left(1 + \frac{\delta_b^2 n_s}{n_b(n_b + \delta_b^2)} \right) \right]^{1/2}, \quad (15)$$

where $\delta_b = x \times n_b$ is the uncertainty on the background yields which is assumed to $x = 5\%$. Moreover we assess the sensitivity reach by computing the expected CL_s [105] using Pyhf [106]. The CL_s estimator is given by

$$\text{CL}_s \equiv \max \left(0, 1 - \frac{p_{b+s}}{p_b} \right), \quad (16)$$

where p_{b+s} and p_b are the signal-plus-background and the background probabilities respectively. In the calculation of the CL_s we assume that the expected number of observed events is equal to the background expectations. Furthermore, we assume that the uncertainty on the background yield is 5%. The results are shown in Fig. 9 where we show the signal significance (left) and CL_s (right) as a function of the DM mass for the resolved and the boosted regimes. We can see that the BDT analysis can probe DM masses up to 1 TeV where both the two statistical prescriptions lead to similar results. We finally the boosted regime has higher sensitivity than the resolved regime as expected.

VI. CONCLUSIONS

In this work we have studied the potential discovery of DM at muon colliders in the mono-Higgs channel. This production channel is very unique in the sense that it would allow the studies of the characteristics of the interactions between the mediator and the SM Higgs sector. As a proof-of-principle we have analysed this channel for the minimal lepton portal DM model which extends the SM with two $SU(2)_L$ singlets: a charged scalar that plays the role of the mediator and a right-handed fermion that assumed to be the DM candidate of the model. After studying the characteristic of the benchmark points allowed by the various constraints, we have studied the production of DM in this channel as well as all the possible backgrounds for center-of-mass energies of 3, 10 and 30 TeV. We have found that the initial signal-to-background ratio for this channel, before any cuts, degrades very quickly with the center-of-mass energy. Therefore, we have analysed the sensitivity reach only for $\sqrt{s} = 3$ TeV and $\mathcal{L} = 1 \text{ ab}^{-1}$. We then performed simple cut-based analysis strategies inspired by the previous ATLAS and CMS searches of DM produced in association with a Higgs boson decaying into bottom quarks. Using different jet clustering algorithms to reconstruct the Higgs boson candidates, we have found poor sensitivities for benchmark points corresponding to heavy DM masses. We have then built an algorithm based on Boosted-Decision Trees (BDT) using XGBOOST library. By optimising the hyperparameters of the models and training it on both the signal and the backgrounds we have found very good improvements by factors of 8–50 with respect to the cut-based analysis. Finally, we have analysed the sensitivity reach by applying this algorithm to the range of DM masses kinematically allowed by the used center-of-mass energy, *i.e.* $M_{NR} \in [50, 1435]$ GeV. We have found that DM masses up to 1 TeV can be excluded at the 95% CL using the BDT analysis and the mono-Higgs channel.

ACKNOWLEDGEMENTS

A.J. would like to thank Jack Araz, Benjamin Fuks and Richard Ruiz for the useful discussions. The work of A.J. is supported by the Institute for Basic Science (IBS) under the project code, IBS-R018-D1. The work of S.N. is supported by the United Arab Emirates University (UAEU) under UPAR Grant No. 12S093.

[1] G. Jungman, M. Kamionkowski, and K. Griest, ‘‘Supersymmetric dark matter,’’ [Phys. Rept. 267 \(1996\) 195–373](#), [arXiv:hep-ph/9506380](#).

- [2] L. Bergström, “Nonbaryonic dark matter: Observational evidence and detection methods,” *Rept. Prog. Phys.* **63** (2000) 793, [arXiv:hep-ph/0002126](#).
- [3] G. Bertone, D. Hooper, and J. Silk, “Particle dark matter: Evidence, candidates and constraints,” *Phys. Rept.* **405** (2005) 279–390, [arXiv:hep-ph/0404175 \[hep-ph\]](#).
- [4] J. L. Feng, “Dark Matter Candidates from Particle Physics and Methods of Detection,” *Ann. Rev. Astron. Astrophys.* **48** (2010) 495–545, [arXiv:1003.0904 \[astro-ph.CO\]](#).
- [5] Planck Collaboration, P. A. R. Ade et al., “Planck 2015 results. XIII. Cosmological parameters,” *Astron. Astrophys.* **594** (2016) A13, [arXiv:1502.01589 \[astro-ph.CO\]](#).
- [6] XENON Collaboration, E. Aprile et al., “Dark Matter Search Results from a One Ton-Year Exposure of XENON1T,” *Phys. Rev. Lett.* **121** (2018) no. 11, 111302, [arXiv:1805.12562 \[astro-ph.CO\]](#).
- [7] PandaX-II Collaboration, X. Cui et al., “Dark Matter Results From 54-Ton-Day Exposure of PandaX-II Experiment,” *Phys. Rev. Lett.* **119** (2017) no. 18, 181302, [arXiv:1708.06917 \[astro-ph.CO\]](#).
- [8] N. Okada and T. Yamada, “Simple fermionic dark matter models and Higgs boson couplings,” *JHEP* **10** (2013) 017, [arXiv:1304.2962 \[hep-ph\]](#).
- [9] K. A. Mohan, D. Sengupta, T. M. P. Tait, B. Yan, and C. P. Yuan, “Direct detection and LHC constraints on a t -channel simplified model of Majorana dark matter at one loop,” *JHEP* **05** (2019) 115, [arXiv:1903.05650 \[hep-ph\]](#).
- [10] G. Belanger et al., “Leptoquark manoeuvres in the dark: a simultaneous solution of the dark matter problem and the $R_{D^{(*)}}$ anomalies,” *JHEP* **02** (2022) 042, [arXiv:2111.08027 \[hep-ph\]](#).
- [11] C. Arina, B. Fuks, J. Heisig, M. Krämer, L. Mantani, and L. Panizzi, “A comprehensive exploration of t -channel simplified models of dark matter,” [arXiv:2307.10367 \[hep-ph\]](#).
- [12] J. Liu, B. Shuve, N. Weiner, and I. Yavin, “Looking for new charged states at the LHC: Signatures of Magnetic and Rayleigh Dark Matter,” *JHEP* **07** (2013) 144, [arXiv:1303.4404 \[hep-ph\]](#).
- [13] Y. Bai and J. Berger, “Lepton Portal Dark Matter,” *JHEP* **08** (2014) 153, [arXiv:1402.6696 \[hep-ph\]](#).
- [14] S. Chang, R. Edezhath, J. Hutchinson, and M. Luty, “Leptophilic Effective WIMPs,” *Phys. Rev. D* **90** (2014) no. 1, 015011, [arXiv:1402.7358 \[hep-ph\]](#).
- [15] M. Garny, A. Ibarra, and S. Vogl, “Signatures of Majorana dark matter with t -channel mediators,” *Int. J. Mod. Phys. D* **24** (2015) no. 07, 1530019, [arXiv:1503.01500 \[hep-ph\]](#).
- [16] A. Jueid, S. Nasri, and R. Soualah, “Searching for GeV-scale Majorana Dark Matter: inter spem et metum,” *JHEP* **04** (2021) 012, [arXiv:2006.01348 \[hep-ph\]](#).
- [17] S.-I. Horigome, T. Katayose, S. Matsumoto, and I. Saha, “Leptophilic fermion WIMP: Role of future lepton colliders,” *Phys. Rev. D* **104** (2021) no. 5, 055001, [arXiv:2102.08645 \[hep-ph\]](#).
- [18] J. Liu, X.-P. Wang, and K.-P. Xie, “Searching for lepton portal dark matter with colliders and gravitational waves,” *JHEP* **06** (2021) 149, [arXiv:2104.06421 \[hep-ph\]](#).
- [19] A. Jueid and S. Nasri, “Lepton portal dark matter at muon colliders: Total rates and generic features for phenomenologically viable scenarios,” *Phys. Rev. D* **107** (2023) no. 11, 115027, [arXiv:2301.12524 \[hep-ph\]](#).
- [20] J. P. Delahaye, M. Diemoz, K. Long, B. Mansoulié, N. Pastrone, L. Rivkin, D. Schulte, A. Skrinsky, and A. Wulzer, “Muon Colliders,” [arXiv:1901.06150 \[physics.acc-ph\]](#).
- [21] K. Long, D. Lucchesi, M. Palmer, N. Pastrone, D. Schulte, and V. Shiltsev, “Muon colliders to expand frontiers of particle physics,” *Nature Phys.* **17** (2021) no. 3, 289–292, [arXiv:2007.15684 \[physics.acc-ph\]](#).
- [22] H. Al Ali et al., “The muon Smasher’s guide,” *Rept. Prog. Phys.* **85** (2022) no. 8, 084201, [arXiv:2103.14043 \[hep-ph\]](#).
- [23] A. Costantini, F. De Lillo, F. Maltoni, L. Mantani, O. Mattelaer, R. Ruiz, and X. Zhao, “Vector boson fusion at multi-TeV muon colliders,” *JHEP* **09** (2020) 080, [arXiv:2005.10289 \[hep-ph\]](#).
- [24] R. Ruiz, A. Costantini, F. Maltoni, and O. Mattelaer, “The Effective Vector Boson Approximation in high-energy muon collisions,” *JHEP* **06** (2022) 114, [arXiv:2111.02442 \[hep-ph\]](#).
- [25] R. Capdevilla, D. Curtin, Y. Kahn, and G. Krnjaic, “Discovering the physics of $(g-2)_\mu$ at future muon colliders,” *Phys. Rev. D* **103** (2021) no. 7, 075028, [arXiv:2006.16277 \[hep-ph\]](#).
- [26] M. Chiesa, F. Maltoni, L. Mantani, B. Mele, F. Piccinini, and X. Zhao, “Measuring the quartic Higgs self-coupling at a multi-TeV muon collider,” *JHEP* **09** (2020) 098, [arXiv:2003.13628 \[hep-ph\]](#).
- [27] T. Han, Y. Ma, and K. Xie, “High energy leptonic collisions and electroweak parton distribution functions,” *Phys. Rev. D* **103** (2021) no. 3, L031301, [arXiv:2007.14300 \[hep-ph\]](#).
- [28] T. Han, Z. Liu, L.-T. Wang, and X. Wang, “WIMPs at High Energy Muon Colliders,” *Phys. Rev. D* **103** (2021) no. 7, 075004, [arXiv:2009.11287 \[hep-ph\]](#).
- [29] W. Yin and M. Yamaguchi, “Muon $g-2$ at a multi-TeV muon collider,” *Phys. Rev. D* **106** (2022) no. 3, 033007, [arXiv:2012.03928 \[hep-ph\]](#).
- [30] G.-y. Huang, F. S. Queiroz, and W. Rodejohann, “Gauged $L_\mu-L_\tau$ at a muon collider,” *Phys. Rev. D* **103** (2021) no. 9, 095005, [arXiv:2101.04956 \[hep-ph\]](#).
- [31] R. Capdevilla, D. Curtin, Y. Kahn, and G. Krnjaic, “No-lose theorem for discovering the new physics of $(g-2)_\mu$ at muon colliders,” *Phys. Rev. D* **105** (2022) no. 1, 015028, [arXiv:2101.10334 \[hep-ph\]](#).

- [32] R. Capdevilla, F. Meloni, R. Simoniello, and J. Zurita, “Hunting wino and higgsino dark matter at the muon collider with disappearing tracks,” *JHEP* **06** (2021) 133, [arXiv:2102.11292 \[hep-ph\]](#).
- [33] P. Asadi, R. Capdevilla, C. Cesarotti, and S. Homiller, “Searching for leptoquarks at future muon colliders,” *JHEP* **10** (2021) 182, [arXiv:2104.05720 \[hep-ph\]](#).
- [34] M. Casarsa, M. Fabbrichesi, and E. Gabrielli, “Monochromatic single photon events at the muon collider,” *Phys. Rev. D* **105** (2022) no. 7, 075008, [arXiv:2111.13220 \[hep-ph\]](#).
- [35] W. Liu, K.-P. Xie, and Z. Yi, “Testing leptogenesis at the LHC and future muon colliders: A Z' scenario,” *Phys. Rev. D* **105** (2022) no. 9, 095034, [arXiv:2109.15087 \[hep-ph\]](#).
- [36] T. Han, S. Li, S. Su, W. Su, and Y. Wu, “Heavy Higgs bosons in 2HDM at a muon collider,” *Phys. Rev. D* **104** (2021) no. 5, 055029, [arXiv:2102.08386 \[hep-ph\]](#).
- [37] T. Han, Y. Ma, and K. Xie, “Quark and gluon contents of a lepton at high energies,” *JHEP* **02** (2022) 154, [arXiv:2103.09844 \[hep-ph\]](#).
- [38] T. Han, W. Kilian, N. Kreher, Y. Ma, J. Reuter, T. Striegl, and K. Xie, “Precision test of the muon-Higgs coupling at a high-energy muon collider,” *JHEP* **12** (2021) 162, [arXiv:2108.05362 \[hep-ph\]](#).
- [39] G.-S. Lv, X.-M. Cui, Y.-Q. Li, and Y.-B. Liu, “Pair production of the vectorlike top partner at future muon collider,” *Nucl. Phys. B* **985** (2022) 116016.
- [40] J. Liu, Z.-L. Han, Y. Jin, and H. Li, “Unraveling the Scotogenic model at muon collider,” *JHEP* **12** (2022) 057, [arXiv:2207.07382 \[hep-ph\]](#).
- [41] A. Azatov, F. Garosi, A. Greljo, D. Marzocca, J. Salko, and S. Trifinopoulos, “New physics in $b \rightarrow s\mu\mu$: FCC-hh or a muon collider?,” *JHEP* **10** (2022) 149, [arXiv:2205.13552 \[hep-ph\]](#).
- [42] J.-C. Yang, X.-Y. Han, Z.-B. Qin, T. Li, and Y.-C. Guo, “Measuring the anomalous quartic gauge couplings in the $W^+W^- \rightarrow W^+W^-$ process at muon collider using artificial neural networks,” *JHEP* **09** (2022) 074, [arXiv:2204.10034 \[hep-ph\]](#).
- [43] Y. Bao, J. Fan, and L. Li, “Electroweak ALP searches at a muon collider,” *JHEP* **08** (2022) 276, [arXiv:2203.04328 \[hep-ph\]](#).
- [44] S. Chen, A. Glioti, R. Rattazzi, L. Ricci, and A. Wulzer, “Learning from radiation at a very high energy lepton collider,” *JHEP* **05** (2022) 180, [arXiv:2202.10509 \[hep-ph\]](#).
- [45] S. Homiller, Q. Lu, and M. Reece, “Complementary signals of lepton flavor violation at a high-energy muon collider,” *JHEP* **07** (2022) 036, [arXiv:2203.08825 \[hep-ph\]](#).
- [46] G.-y. Huang, S. Jana, F. S. Queiroz, and W. Rodejohann, “Probing the $RK^{(*)}$ anomaly at a muon collider,” *Phys. Rev. D* **105** (2022) no. 1, 015013, [arXiv:2103.01617 \[hep-ph\]](#).
- [47] S. Sun, Q.-S. Yan, X. Zhao, and Z. Zhao, “Constraining rare B decays by $\mu^+\mu^- \rightarrow tc$ at future lepton colliders,” [arXiv:2302.01143 \[hep-ph\]](#).
- [48] S. Zhang, J.-C. Yang, and Y.-C. Guo, “Using k-means assistant event selection strategy to study anomalous quartic gauge couplings at muon colliders,” [arXiv:2302.01274 \[hep-ph\]](#).
- [49] J.-L. Yang, C.-H. Chang, and T.-F. Feng, “The leptonic di-flavor and di-number violation processes at high energy $\mu^\pm\mu^\pm$ colliders,” [arXiv:2302.13247 \[hep-ph\]](#).
- [50] F. Garosi, D. Marzocca, and S. Trifinopoulos, “LePDF: Standard Model PDFs for high-energy lepton colliders,” *JHEP* **09** (2023) 107, [arXiv:2303.16964 \[hep-ph\]](#).
- [51] Y.-F. Dong, Y.-C. Mao, and J.-C. Yang, “Searching for anomalous quartic gauge couplings at muon colliders using principal component analysis,” *Eur. Phys. J. C* **83** (2023) no. 7, 555, [arXiv:2304.01505 \[hep-ph\]](#).
- [52] K. Fridell, R. Kitano, and R. Takai, “Lepton flavor physics at $\mu^+\mu^+$ colliders,” *JHEP* **06** (2023) 086, [arXiv:2304.14020 \[hep-ph\]](#).
- [53] T. A. Chowdhury, A. Jueid, S. Nasri, and S. Saad, “Probing Zee-Babu states at Muon Colliders,” [arXiv:2306.01255 \[hep-ph\]](#).
- [54] A. Belyaev, R. S. Chivukula, B. Fuks, E. H. Simmons, and X. Wang, “Vectorlike top quark production via an electroweak dipole moment at a muon collider,” *Phys. Rev. D* **108** (2023) no. 3, 035016, [arXiv:2306.11097 \[hep-ph\]](#).
- [55] J.-C. Yang, Y.-C. Guo, and Y.-F. Dong, “Study of the gluonic quartic gauge couplings at muon colliders,” [arXiv:2307.04207 \[hep-ph\]](#).
- [56] M. Belfkir, T. A. Chowdhury, and S. Nasri, “Doubly-charged scalars of the Minimal Left-Right Symmetric Model at Muon Colliders,” [arXiv:2307.16111 \[hep-ph\]](#).
- [57] M. Forslund and P. Meade, “Precision Higgs Width and Couplings with a High Energy Muon Collider,” [arXiv:2308.02633 \[hep-ph\]](#).
- [58] Z. Liu, K.-F. Lyu, I. Mahbub, and L.-T. Wang, “Top Yukawa Coupling Determination at High Energy Muon Collider,” [arXiv:2308.06323 \[hep-ph\]](#).
- [59] S. Jana and S. Klett, “Muonic Force and Neutrino Non-Standard Interactions at Muon Colliders,” [arXiv:2308.07375 \[hep-ph\]](#).
- [60] A. Dasgupta, P. S. B. Dev, T. Han, R. Padhan, S. Wang, and K. Xie, “Searching for Heavy Leptophilic Z' : from Lepton Colliders to Gravitational Waves,” [arXiv:2308.12804 \[hep-ph\]](#).

- [61] N. Ghosh, S. K. Rai, and T. Samui, “Search For a Leptoquark and Vector-like Lepton in a Muon Collider,” [arXiv:2309.07583 \[hep-ph\]](#).
- [62] B. A. Ouazghour, A. Arhrib, K. Cheung, E.-s. Ghourmin, and L. Rahili, “Charged Higgs production at the Muon Collider in the 2HDM,” [arXiv:2308.15664 \[hep-ph\]](#).
- [63] S. Frixione and G. Stagnitto, “The muon parton distribution functions,” [arXiv:2309.07516 \[hep-ph\]](#).
- [64] L. Carpenter, A. DiFranzo, M. Mulhearn, C. Shimmin, S. Tulin, and D. Whiteson, “Mono-Higgs-boson: A new collider probe of dark matter,” [Phys. Rev. D **89** \(2014\) no. 7, 075017](#), [arXiv:1312.2592 \[hep-ph\]](#).
- [65] A. Berlin, T. Lin, and L.-T. Wang, “Mono-Higgs Detection of Dark Matter at the LHC,” [JHEP **06** \(2014\) 078](#), [arXiv:1402.7074 \[hep-ph\]](#).
- [66] J. M. No, “Looking through the pseudoscalar portal into dark matter: Novel mono-Higgs and mono-Z signatures at the LHC,” [Phys. Rev. D **93** \(2016\) no. 3, 031701](#), [arXiv:1509.01110 \[hep-ph\]](#).
- [67] W. Abdallah, A. Hammad, S. Khalil, and S. Moretti, “Search for Mono-Higgs Signals at the LHC in the B-L Supersymmetric Standard Model,” [Phys. Rev. D **95** \(2017\) no. 5, 055019](#), [arXiv:1608.07500 \[hep-ph\]](#).
- [68] K. Ghorbani and L. Khalkhali, “Mono-Higgs signature in a fermionic dark matter model,” [J. Phys. G **44** \(2017\) no. 10, 105004](#), [arXiv:1608.04559 \[hep-ph\]](#).
- [69] L. Basso, “Resonant mono Higgs at the LHC,” [JHEP **04** \(2016\) 087](#), [arXiv:1512.06381 \[hep-ph\]](#).
- [70] S. Antusch, E. Cazzato, and O. Fischer, “Higgs production from sterile neutrinos at future lepton colliders,” [JHEP **04** \(2016\) 189](#), [arXiv:1512.06035 \[hep-ph\]](#).
- [71] A. A. Petrov and W. Shepherd, “Searching for dark matter at LHC with Mono-Higgs production,” [Phys. Lett. B **730** \(2014\) 178–183](#), [arXiv:1311.1511 \[hep-ph\]](#).
- [72] S. Baum, K. Freese, N. R. Shah, and B. Shakya, “NMSSM Higgs boson search strategies at the LHC and the mono-Higgs signature in particular,” [Phys. Rev. D **95** \(2017\) no. 11, 115036](#), [arXiv:1703.07800 \[hep-ph\]](#).
- [73] A. Ahriche, A. Arhrib, A. Jueid, S. Nasri, and A. de La Puente, “Mono-Higgs Signature in the Scotogenic Model with Majorana Dark Matter,” [Phys. Rev. D **101** \(2020\) no. 3, 035038](#), [arXiv:1811.00490 \[hep-ph\]](#).
- [74] S. Argyropoulos, O. Brandt, and U. Haisch, “Collider Searches for Dark Matter through the Higgs Lens,” [Symmetry **13** \(2021\) no. 12, 2406](#), [arXiv:2109.13597 \[hep-ph\]](#).
- [75] A. Hammad, S. Khalil, and S. Moretti, “Search for mono-Higgs signals in bb^- final states using deep neural networks,” [Phys. Rev. D **107** \(2023\) no. 7, 075027](#), [arXiv:2208.10133 \[hep-ph\]](#).
- [76] S. Banerjee, G. Bélanger, D. Bhatia, B. Fuks, and S. Raychaudhuri, “Phenomenological analysis of multi-pseudoscalar mediated dark matter models,” [JHEP **07** \(2022\) 111](#), [arXiv:2110.15391 \[hep-ph\]](#).
- [77] D. Bhowmik, J. Lahiri, S. Bhattacharya, B. Mukhopadhyaya, and R. K. Singh, “The mono-Higgs + MET signal at the Large Hadron Collider: a study on the $\gamma\gamma$ and bb final states,” [Eur. Phys. J. C **82** \(2022\) no. 10, 914](#), [arXiv:2012.07822 \[hep-ph\]](#).
- [78] **ATLAS** Collaboration, G. Aad et al., “Search for dark matter produced in association with a Standard Model Higgs boson decaying into b-quarks using the full Run 2 dataset from the ATLAS detector,” [JHEP **11** \(2021\) 209](#), [arXiv:2108.13391 \[hep-ex\]](#).
- [79] **CMS** Collaboration, A. M. Sirunyan et al., “Search for dark matter produced in association with a Higgs boson decaying to a pair of bottom quarks in proton–proton collisions at $\sqrt{s} = 13$ TeV,” [Eur. Phys. J. C **79** \(2019\) no. 3, 280](#), [arXiv:1811.06562 \[hep-ex\]](#).
- [80] J. Alwall, R. Frederix, S. Frixione, V. Hirschi, F. Maltoni, O. Mattelaer, H. S. Shao, T. Stelzer, P. Torrielli, and M. Zaro, “The automated computation of tree-level and next-to-leading order differential cross sections, and their matching to parton shower simulations,” [JHEP **07** \(2014\) 079](#), [arXiv:1405.0301 \[hep-ph\]](#).
- [81] C. Degrande, C. Duhr, B. Fuks, D. Grellscheid, O. Mattelaer, and T. Reiter, “UFO - The Universal FeynRules Output,” [Comput. Phys. Commun. **183** \(2012\) 1201–1214](#), [arXiv:1108.2040 \[hep-ph\]](#).
- [82] A. Alloul, N. D. Christensen, C. Degrande, C. Duhr, and B. Fuks, “FeynRules 2.0 - A complete toolbox for tree-level phenomenology,” [Comput. Phys. Commun. **185** \(2014\) 2250–2300](#), [arXiv:1310.1921 \[hep-ph\]](#).
- [83] C. Bierlich et al., “A comprehensive guide to the physics and usage of PYTHIA 8.3,” [arXiv:2203.11601 \[hep-ph\]](#).
- [84] M. Cacciari, G. P. Salam, and G. Soyez, “The Anti-k(t) jet clustering algorithm,” [JHEP **04** \(2008\) 063](#), [arXiv:0802.1189 \[hep-ph\]](#).
- [85] D. Krohn, J. Thaler, and L.-T. Wang, “Jet Trimming,” [JHEP **02** \(2010\) 084](#), [arXiv:0912.1342 \[hep-ph\]](#).
- [86] S. Catani, Y. L. Dokshitzer, M. H. Seymour, and B. R. Webber, “Longitudinally invariant K_t clustering algorithms for hadron hadron collisions,” [Nucl. Phys. B **406** \(1993\) 187–224](#).
- [87] **CMS** Collaboration, “A Cambridge-Aachen (C-A) based Jet Algorithm for boosted top-jet tagging.”
- [88] A. J. Larkoski, S. Marzani, G. Soyez, and J. Thaler, “Soft Drop,” [JHEP **05** \(2014\) 146](#), [arXiv:1402.2657 \[hep-ph\]](#).
- [89] I. Moult, L. Necib, and J. Thaler, “New Angles on Energy Correlation Functions,” [JHEP **12** \(2016\) 153](#), [arXiv:1609.07483 \[hep-ph\]](#).
- [90] J. Y. Araz, B. Fuks, and G. Polykratis, “Simplified fast detector simulation in MADANALYSIS 5,” [Eur. Phys. J. C **81** \(2021\) no. 4, 329](#), [arXiv:2006.09387 \[hep-ph\]](#).

- [91] E. Conte, B. Fuks, and G. Serret, “MadAnalysis 5, A User-Friendly Framework for Collider Phenomenology,” *Comput. Phys. Commun.* **184** (2013) 222–256, [arXiv:1206.1599 \[hep-ph\]](#).
- [92] B. Dumont, B. Fuks, S. Kraml, S. Bein, G. Chalons, E. Conte, S. Kulkarni, D. Sengupta, and C. Wymant, “Toward a public analysis database for LHC new physics searches using MADANALYSIS 5,” *Eur. Phys. J. C* **75** (2015) no. 2, 56, [arXiv:1407.3278 \[hep-ph\]](#).
- [93] E. Conte, B. Dumont, B. Fuks, and C. Wymant, “Designing and recasting LHC analyses with MadAnalysis 5,” *Eur. Phys. J. C* **74** (2014) no. 10, 3103, [arXiv:1405.3982 \[hep-ph\]](#).
- [94] E. Conte and B. Fuks, “Confronting new physics theories to LHC data with MADANALYSIS 5,” *Int. J. Mod. Phys. A* **33** (2018) no. 28, 1830027, [arXiv:1808.00480 \[hep-ph\]](#).
- [95] J. Y. Araz, M. Frank, and B. Fuks, “Reinterpreting the results of the LHC with MadAnalysis 5: uncertainties and higher-luminosity estimates,” *Eur. Phys. J. C* **80** (2020) no. 6, 531, [arXiv:1910.11418 \[hep-ph\]](#).
- [96] J. Y. Araz, B. Fuks, M. D. Goodsell, and M. Utsch, “Recasting LHC searches for long-lived particles with MadAnalysis 5,” *Eur. Phys. J. C* **82** (2022) no. 7, 597, [arXiv:2112.05163 \[hep-ph\]](#).
- [97] J. Y. Araz, A. Buckley, and B. Fuks, “Searches for new physics with boosted top quarks in the MadAnalysis 5 and Rivet frameworks,” [arXiv:2303.03427 \[hep-ph\]](#).
- [98] M. Cacciari, G. P. Salam, and G. Soyez, “FastJet User Manual,” *Eur. Phys. J. C* **72** (2012) 1896, [arXiv:1111.6097 \[hep-ph\]](#).
- [99] **DELPHES 3** Collaboration, J. de Favereau, C. Delaere, P. Demin, A. Giammanco, V. Lemaître, A. Mertens, and M. Selvaggi, “DELPHES 3, A modular framework for fast simulation of a generic collider experiment,” *JHEP* **02** (2014) 057, [arXiv:1307.6346 \[hep-ex\]](#).
- [100] **Muon Collider** Collaboration, N. Bartosik et al., “Simulated Detector Performance at the Muon Collider,” [arXiv:2203.07964 \[hep-ex\]](#).
- [101] E. Bernreuther, J. Horak, T. Plehn, and A. Butter, “Actual Physics behind Mono-X,” *SciPost Phys.* **5** (2018) no. 4, 034, [arXiv:1805.11637 \[hep-ph\]](#).
- [102] G. Cowan, K. Cranmer, E. Gross, and O. Vitells, “Asymptotic formulae for likelihood-based tests of new physics,” *Eur. Phys. J. C* **71** (2011) 1554, [arXiv:1007.1727 \[physics.data-an\]](#). [Erratum: *Eur. Phys. J. C* **73**, 2501 (2013)].
- [103] F. Pedregosa, G. Varoquaux, A. Gramfort, V. Michel, B. Thirion, O. Grisel, M. Blondel, P. Prettenhofer, R. Weiss, V. Dubourg, J. Vanderplas, A. Passos, D. Cournapeau, M. Brucher, M. Perrot, and E. Duchesnay, “Scikit-learn: Machine learning in Python,” *Journal of Machine Learning Research* **12** (2011) 2825–2830.
- [104] T. Chen and C. Guestrin, “XGBoost,” in *Proceedings of the 22nd ACM SIGKDD International Conference on Knowledge Discovery and Data Mining*. ACM, aug, 2016. <https://doi.org/10.1145/2F2939672.2939785>.
- [105] A. L. Read, “Presentation of search results: The CL(s) technique,” *J. Phys. G* **28** (2002) 2693–2704. [11(2002)].
- [106] L. Heinrich, M. Feickert, G. Stark, and K. Cranmer, “pyhf: pure-python implementation of histfactory statistical models,” *Journal of Open Source Software* **6** (2021) no. 58, 2823. <https://doi.org/10.21105/joss.02823>.